analytical chemistry

Article

pubs.acs.org/ac

Highly Efficient Visual Detection of Trace Copper(II) and Protein by the Quantum Photoelectric Effect

Peng Wang, Jianping Lei, Mengqi Su, Yueting Liu, Qing Hao, and Huangxian Ju*

State Key Laboratory of Analytical Chemistry for Life Science, Department of Chemistry, Nanjing University, Nanjing 210093, China

ABSTRACT: This work presented a photocurrent response mechanism of quantum dots (QDs) under illumination with the concept of a quantum photoelectric effect. Upon irradiation, the photoelectron could directly escape from QDs. By using nitro blue tetrazolium (NBT) to capture the photoelectron, a new visual system was proposed due to the formation of an insoluble reduction product, purple formazan, which could be used to visualize the quantum photoelectric effect. The interaction of copper(II) with QDs could form trapping sites to interfere with the quantum confinement and thus blocked the escape of photoelectron, leading to a "signal off" visual method for sensitive copper(II) detection. Meanwhile, by using QDs as a signal tag to label antibody, a "signal on" visual method was also proposed for immunoassay of corresponding protein. With *meso*-2,3-dimercaptosuccinic-capped CdTe QDs and carcino-embryonic antigen as models, the proposed visual detection methods showed high sensitivity, low detection limit, and wide detectable concentration ranges. The visualization of quantum photoelectric effect could be simply extended for the detection of other targets. This work opens a new visual detection way and provides a highly efficient tool for bioanalysis.

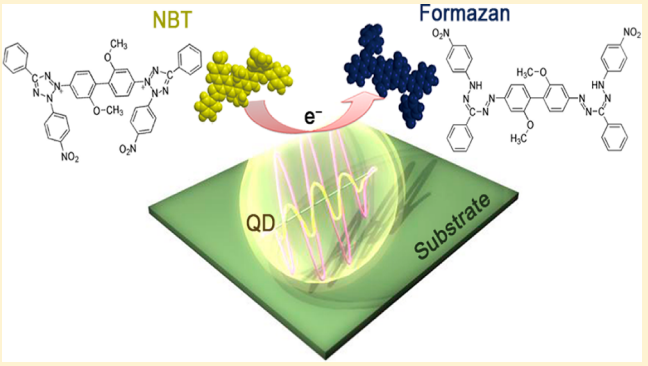

The quantum effect of nanoparticles results in their unique optical and electrical properties[1,2] that provide the basis of various applications of nanoparticles in solar energy conversion devices and ultrasensitive sensors.[3−6] Quantum dots (QDs), as a kind of representative nanoparticle, are able to generate photoelectrons under irradiation,[4,5] and the escape of those photoelectrons is closely related to the energy states of QDs. As the precursor of photoelectron, the exciton, produced from the QDs under irradiation,[4] is spatially restricted by the quantum confinement,[7−9] which results in a narrow distribution and fewer futile loss of the energy;[10] thus, the phenomenon of quantum efficiency exceeding 100% in QDs has even been observed.[11] The circumstantial alternation can sensitively change the quantum states of the QDs, which is reflected in the exciton states, leading to the status change of the photoelectron. Thus, the escape of photoelectrons is actually controlled by the quantum confinement of QDs. As a result, the photoelectrochemical response of QDs to the alternation of the circumstance is more sensitive compared with the bulk semiconductor materials. Previously, we reported the observation of cathode photocurrent of QDs due to the formation of exciton and its decrease in the presence of copper ion due to the interaction of copper ion with QDs to trap the exciton.[4] On the basis of the spectroscopic characterization, this work presented the concept of the quantum photoelectric effect, which can be defined as the photoinduced electric response of a quantum unit, and the exciton or excited electrons can interact with another basic unit such as a small molecule, ion, or atom to produce the energy transformation or the photocurrent alternation.

The quantum photoelectric effect leads to the production of a high-energy photoelectron. The escaped photoelectron can inject into the orbital of dissolved oxygen to produce supper oxide radical ($O_2^{-\bullet}$),[12−15] which induces us to search for an electron acceptor of $O_2^{-\bullet}$ to capture the photoelectron for developing analytical methodology. As an acceptor of $O_2^{-\bullet}$,[16−23] nitro blue tetrazolium (NBT) is thus selected to be added in the photoelectrochemical system. Incidentally, after NBT accepts the electrons, an insoluble purple compound is formed, which produces a new visual method to monitor the photoelectron transfer. Thus, a sensitive method is proposed for visualization of the quantum states of the QDs and quantum photoelectric effect. Furthermore, the visual response is unrelated to the presence of dissolved oxygen, indicating that the escaped photoelectron can directly inject into the orbital of NBT.

Now that the interaction of copper ion with QDs produces the trapping sites[24−27] to trap the exciton[4] and thus block the escape of photoelectrons,[27] the formation of purple formazan can be hindered. As a proof-of-concept, a visual method was developed for "signal off" detection of copper ion. This method showed a quick and sensitive response to trace copper(II). The detectable concentration range was even wider than those

Received: June 11, 2013
Accepted: August 21, 2013
Published: August 21, 2013

performed with different instruments such as a photoelectrochemical analyzer,[27] fluorescence analyzer,[28] atomic absorption spectrometer,[29] and voltammeter.[30] The analytical performance was also better than previously reported visual methods based on click chemistry and functional gold nanoparticles.[31,32]

Different from the electrochemiluminescent and photoelectrochemical detection, the visual detection does not involve the electron transfer between QDs and electrode, which greatly depends on the surface state of electrode, limits the distance between QDs and electrode, and is thus more suitable to homogeneous detection or monitoring the multistep recognition reactions. As an example, the proposed visual system was further used for "signal on" immunoassay by labeling the secondary antibody with QDs and simply immobilizing the capture antibody on a glass substrate. Using carcino-embryonic antigen (CEA) as a model analyte of the sandwich immunoassay, the designed visual method could detect CEA down to 0.02 ng/mL, which was about 20 times lower than 0.39 ng/mL of conventional ELISA method.[33] The low cost and convenient manipulation of the visual method indicated a potential application in detection of disease biomarkers.

EXPERIMENTAL SECTION

Materials and Reagents. *meso*-2,3-Dimercaptosuccinic acid (DMSA) and cadmium chloride ($CdCl_2 \cdot 2.5H_2O$) were purchased from Alfa Aesar China Ltd. Tellurium rod (4 mm in diameter) was purchased from Leshan Kayada Photoelectricity Co., Ltd. Cupric nitrate [$Cu(NO_3)_2 \cdot 3H_2O$] was purchased from Shanghai Sinpeuo Fine Chemical Co., Ltd. NBT was purchased from Shengxing Biotechnology Ltd. 5,5-Dimethyl-1-pyrroline *N*-oxide (DMPO) was purchased from Sigma-Aldrich Inc. and dissolved in 0.1 M pH 7.4 phosphate-buffered saline (PBS). 1-Ethyl-3-(3-dimethylaminopropyl) carbodiimide (EDC) and *N*-hydroxysuccinimide (NHS) were purchased from Sigma-Aldrich Inc. CEA enzyme-linked immuno sorbent assay (ELISA) kit containing CEA standard solutions and washing buffer was purchased from Fujirebio Diagnostics, Inc. Anti-CEA antibody was purchased from Boson Biotech Co., Ltd. Amino-coated glass slides were obtained from Shanghai BaiO Technology Co., Ltd. All the other chemicals were of analytical grade without further purification. All aqueous solutions were prepared using ultrapure water obtained from a Millipore water purification system (≥18 MΩ, Milli-Q, Millipore).

Synthesis of DMSA-Capped CdTe QDs. The DMSA-capped CdTe QDs were synthesized with an electrolysis method reported previously[34] using a CHI 660D electrochemical workstation (CH Instruments Inc.). First, 6.5 mg of DMSA, 200 μL of 1 M NaOH, and 120 μL of 0.1 M $CdCl_2$ were added into 20 mL of water in sequence. After being bubbled with highly pure N_2 for 20 min, this solution was used as electrolyte by applying a constant potential of −1.0 V (vs saturated calomel electrode) on a Te electrode until an electric charge of 0.5 C was reached. During the electrolysis process, the solution was continuously bubbled with highly pure N_2. After the resulting solution was refluxed at 50 °C for 24 h, an equal volume of isopropyl alcohol was added, and the mixture was centrifuged at 8000 rpm for 5 min. The obtained precipitate was washed with a 1:1 mixture of isopropyl alcohol and water and then redissolved in 20 mL of water, which was kept at 4 °C prior to use. After storage for 2 months, the solution remained clear and stable.

Preparation of QDs Labeled Antibody and Antibody Immobilized Substrate. A 300 μL portion of NHS solution (3.8 mg/mL) and 400 μL of the prepared QDs solution were sequentially added into 200 μL of EDC (50 mg/mL in 0.01 M PBS). After reaction at room temperature for 10 min, 400 μL of 0.5 mg/mL anti-CEA was added into the mixture. The obtained solution was shocked for 30 min away from light and then set at 4 °C overnight.

An amino-coated glass slide was immersed in 12.5% glutaraldehyde solution overnight away from light. After washing with water and drying in air, 20 μL of anti-CEA antibody solution (10 μg/mL in pH 9−10 solution of 1.5 mg/mL Na_2CO_3 and 2.4 mg/mL $NaHCO_3$[35]) was dropped on to the slide to form a detecting point. After the needed points were dropped, the glass slide was put under 37 °C for 1 h and 4 °C overnight.[36] The extra antibody was washed away with the washing buffer.

Visualization Process. Ten microliters of the obtained QDs solution was mixed with 10 μL of 1.0 mg/mL NBT on a glass substrate. The mixture was then set under irradiation of a white light of ca. 60 000 lx to observe the color change. To understand the role of O_2 in the reaction, 100 μL of QDs and 100 μL of 1.0 mg/mL NBT were mixed in a tube to observe the color change under light after the mixture was saturated with N_2.

To study the reaction mechanism, an EMX-10/12 electronic paramagnetic resonance (EPR) spectrometer with a mercury lamp (Heraeus fur Strahler Q180, Bruker) was used to record the EPR spectra during the reaction in the presence and absence of dissolved oxygen. The effect of wavelength on photoelectric reaction was examined by using an intensity modulated photospectrometer with light-emitting diodes (Zahner) to control the strength and wavelength of illumination. The X-ray photoelectron spectra (XPS) was recorded with a PHI5000 VersaProbe X-ray photoelectron spectrometer (ULVAC-PHI Co.). Fluorescence and UV−vis spectra were obtained on a RF-5301 PC luminescence spectrometer (Shimadzu) and a UV-3600 UV−vis−NIR spectrometer (Shimadzu), respectively. All photographs were taken with a DSC-TX100 camera (Sony).

Visual Detection of Trace Copper(II) and CEA. After 10 μL of Cu^{2+} solution at a certain concentration or sample was mixed with 10 μL of the obtained QDs solution and 10 μL of 1.0 mg/mL NBT on a glass slide kept away from light, the glass slide was immediately set under white light of 60 000 lx for a selected time. The color change was detected by the naked eye or from its photograph with the help of Adobe Photoshop software. With the histogram function in Photoshop, the color values in cyan-blue and yellow channels could be read out respectively to obtain their difference, which was used to determine the concentration of Cu^{2+}. To investigate the ability of the visual method against interference of other ions, the visualization process was also carried out in the presence of different metal cations.

The sandwich immunoassay was performed by dropping 20 μL of CEA solution or sample onto the detecting point and incubating at room temperature for 10 min, followed with washing and dropping of 20 μL of QD-labeled antibody to incubate for 1 h. After being washed with washing buffer and dried in nitrogen stream, 20 μL of 1.0 mg/mL NBT was dropped onto each point and exposed to white light of ca. 60 000 lx for 10 min to read out the color change. The quantification could be performed with the magic stick tool of

dx.doi.org/10.1021/ac401749u | Anal. Chem. 2013, 85, 8735−8740

Photoshop software to get the area percentage of the dark points appeared in the total area, which could be used to determine the concentration of CEA. During the detection process, deaeration was unnecessary.

RESULTS AND DISCUSSION

Visualization Reaction. Under illumination of ca. 60 000 lx white light, the color of the mixture of QDs and NBT changed from yellow to purple within 1 min. With the increasing irradiation density and amounts of NBT and QDs, the rate of color change became faster, and the eventual color was also darker. According to the previous reports, NBT is well-known as the electron acceptor of $O_2^{-\bullet}$,[16−23] which results in the production of purple formazan. Thus, NBT has been widely used to evaluate the activities of enzymes, or to screen the radioprotective activity of plant species, since $O_2^{-\bullet}$ acts as the intermediate of various enzyme reactions or photochemical reactions.[21,23] Meanwhile, the excitation of QDs by illumination in the presence of dissolved oxygen can lead to the formation of $O_2^{-\bullet}$.[4,14,15] Therefore, the reduction of NBT by QDs under illumination is probably via $O_2^{-\bullet}$ as an intermediate. However, this work interestingly found that the color change of NBT/QDs solution corresponding to the reduction of NBT could occur in the absence of dissolved oxygen. Under illumination, no obvious difference in the discoloration was observed in the presence and absence of O_2, which excluded the help of $O_2^{-\bullet}$. The result was proved with EPR spectra, indicating a direct photoelectron-accepting reaction path between NBT and QDs (Scheme 1A).

Scheme 1. Schematic Illustration of the Visualization of Quantum Photoelectric Effect (A), Copper Ion (B), and Immunoassay (C)[a]

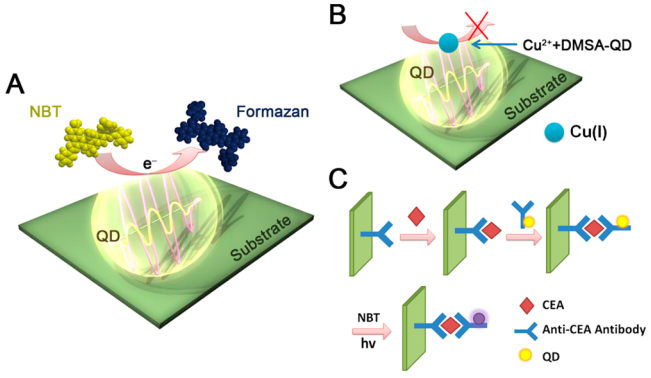

[a]The semitransparent ball denotes DMSA-capped CdTe QDs; the sinusoidal curves denote the ground electronic energy state (yellow) and the excited electronic energy state (pink); the curved arrow denotes the way that NBT gains the photoelectrons.

DMPO is a generally used capture of $O_2^{-\bullet}$ to characterize the presence of $O_2^{-\bullet}$ by EPR spectrum, which shows six sharp hyperfine split peaks of DMPO−OOH, the reaction product of DMPO and $O_2^{-\bullet}$,[16,37] with a half-life of 66 s.[38] In this work, the EPR spectra of the mixtures of DMPO with air-saturated QDs, NBT, and QDs/NBT did not show the six specific peaks during illumination for 5 min (Figure 1a). Different from the mixture of QDs and DMPO (curve 1), the mixture of NBT and DMPO displayed four other peaks at 3450, 3465, 3480, and 3495 G with an intensity ratio of 1:2:2:1 (curve 2), which were attributed to hydroxyl radicals ($OH^{\bullet}$).[37] In the coexistence of

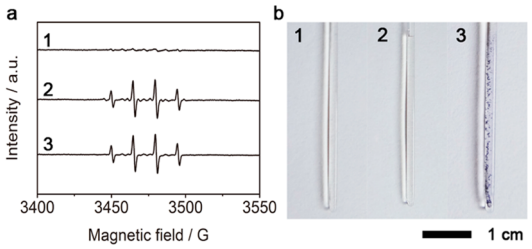

Figure 1. (a) EPR spectra and (b) photographs of QDs (1), NBT (2), and the mixture of QDs and NBT (3) in presence of DMPO during irradiation with white light of ca. 72 000 lx for 5 min.

QDs and NBT, the irradiation also produced the $OH^{\bullet}$ peaks (curve 3). Thus, the production of $OH^{\bullet}$ was possibly related to the illuminated NBT. In the mixture of QDs and DMPO, the EPR spectrum did not show the presence of both $O_2^{-\bullet}$ and $OH^{\bullet}$ during the illumination, indicating the absence of DMPO−OOH or $O_2^{-\bullet}$. Further results indicated that the production of $OH^{\bullet}$ in NBT solution did not change its color (Figure 1b, photograph 2). Although the EPR peaks of NBT solution and QDs/NBT mixture occurred at the same positions and showed the same appearance, the mixture of QDs and NBT showed an obvious change in color (Figure 1b, photograph 3), which corresponded to the reduction of NBT to produce formazan. Thus, $OH^{\bullet}$ did not participate in the discoloration, and the formation of $O_2^{-\bullet}$ was not a necessary condition for the reduction process. The reduction of NBT should be directly related to the photoelectric effect of QDs, which led to the escape of photoelectrons to inject into the orbital of NBT. This process could be described with the following equation:

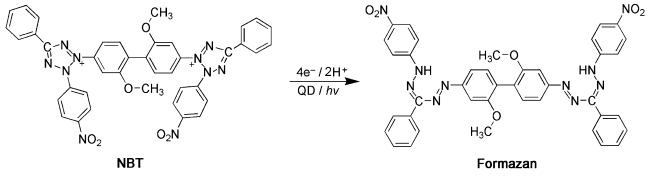

This reaction produces purple formazan (Figure 1b, photograph 3), realizing the visualization of the photoelectric response of QDs under illumination.

Visualization of Quantum Photoelectric Effect. By applying the visualization reaction, the photoelectric response mechanism was further studied. Under illumination the excitons produced in QDs are spatially restricted by a three-dimensional potential well.[8] As a result, the states of the excitons are controlled by the well lengths.[9,25] Hence, the photoelectric response of QDs should depend on the particle size, which can be controlled by the reflux time used in QD synthesis[39] and can be read out via the visualization reaction with the help of NBT. With the increasing reflux time, the absorption peak of the UV−vis spectrum of the obtained QDs red-shifted, indicating that the increasing size of the QDs and length of the potential well restricted the excitons, which led to different quantum states.[10,39] The QDs with different quantum states should produce different responses to the same excitation. Using the QDs obtained with reflux for 0, 2, and 24 h as examples, their UV−vis spectra and the photographs of the mixtures of corresponding QDs and NBT after illumination with a light emitting diode (LED) at 453 ± 13 and 529 ± 21 nm are shown in Figure 2.

dx.doi.org/10.1021/ac401749u | Anal. Chem. 2013, 85, 8735−8740

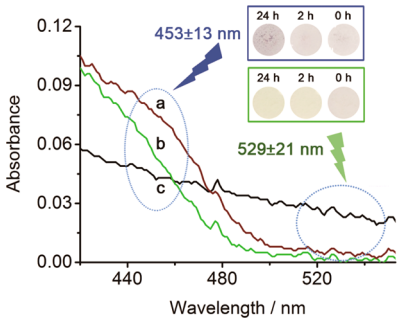

Figure 2. UV−vis spectra of QDs obtained with reflux for 24, 2, and 0 h (from a to c). Inset: spots for the mixtures of corresponding QDs and NBT after illumination at 453 ± 13 nm (upper) and 529 ± 21 nm (below) for 2 min.

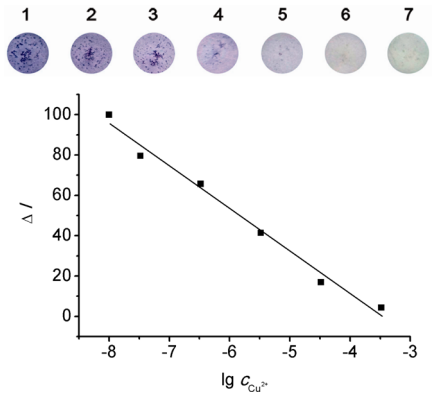

Figure 3. Spots for the mixtures of QDs and NBT in presence of 0, 1.0 × 10^{-8}, 3.3 × 10^{-8}, 3.3 × 10^{-7}, 3.3 × 10^{-6}, 3.3 × 10^{-5}, and 3.3 × 10^{-4} M Cu^{2+} (from 1 to 7) after illumination with white light of ca. 60 000 lx for 5 min and a plot of difference between the intensities (ΔI) read from cyan-blue and yellow channels with Adobe Photoshop software vs logarithm of Cu^{2+} concentration.

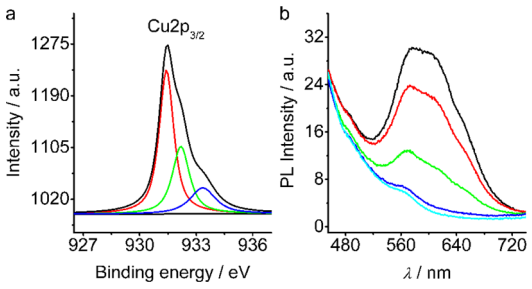

Figure 4. (a) XPS spectrum of Cu2p in the mixture of Cu^{2+} and QDs. The main peak was fitted into three subpeaks at 931.4, 932.2, and 933.4 eV. (b) Fluorescence emission spectra of QDs solutions containing 0, 3.3 × 10^{-8}, 3.3 × 10^{-7}, 3.3 × 10^{-6}, and 3.3 × 10^{-5} M Cu^{2+} (from up to bottom). The excitation wavelength was 390 nm.

Under irradiation at 453 ± 13 nm, the mixture of NBT and QDs with reflux for 24 h changed its color from yellow to purple within 1 min, while the mixture of NBT and QDs with reflux for 0 and 2 h did not show any color change until 2 min. This appearance resulted from the fact that the QDs with reflux for 24 h possessed larger well size of exciton and thus the lower excitation energy, which led to more excitons due to the stronger absorption in the region of 453 ± 13 nm than the other two kinds of QDs (Figure 2). After irradiation for 2 min at 529 ± 21 nm, which is not the characteristic adsorption wavelength of these QDs, only the spot for QDs with reflux for 0 h showed slight change in its color, which resulted from the greater adsorption of the QDs (curve c). Thus, the color changes at different conditions were closely related to the quantum states of QDs, reflecting that the photoelectric response of QDs was controlled by the quantum confinement, inducing the concept of the quantum photoelectric effect. The excitons controlled by quantum confinement possess highly concentrated energy and are sensitive to the alternation of the quantum states, providing a promising platform for design of advanced and convenient visual sensors.

"Signal off" Visual Detection of Trace Copper. As an example, a visual sensor for highly efficient detection of trace Cu^{2+} was designed here to verify the usage of the visualization of the quantum photoelectric effect (Scheme 1B). Upon addition of Cu^{2+}, the quantum photoelectric effect of QDs alternated due to the interaction of QDs with Cu^{2+}. With the increasing concentration of Cu^{2+} from 1.0 × 10^{-8} to 3.3 × 10^{-4} M, the color change lowered, leading to the spot color change from dark purple to light purple to yellow (Figure 3).

XPS and fluorescence spectra were used to illustrate the interaction between QDs with Cu^{2+} and the alternation of quantum photoelectric effect of the QDs (Figure 4). After interaction with QDs, the binding energy of $Cu2p_{3/2}$ split into three parts with peak values of 931.4, 932.2, and 933.4 eV, respectively (Figure 4a). As reported in the previous work,[4,40,41] the peak at 931.4 eV resulted from Cu(I), which was produced from the interaction between Cu^{2+} and thiol groups on the surface of QDs and played an important role in altering the quantum state of the QDs.[4,23,24] The redox energy level of Cu^{I} sits between the valence band and the conduction band of the QDs, leading to the change of quantum effect and the formation of the trapping sites.[27] The trapping sites resisted the formation of the exciton and thus the photoelectron for reducing NBT. The decrease in number of the photoelectrons could be illustrated by the decreasing cathode photocurrent response of QDs as the amount of copper ion increased.[4] At the same time, the decreasing number of excitons could be observed from the weakening fluorescence intensity of the QDs with the increasing concentration of Cu^{2+} in QDs solution (Figure 4b). Since the excitons and photoelectrons play a critical role in quantum photoelectric effect, both the decreasing photocurrent and the decreasing fluorescence intensity demonstrated that the color change corresponding to the different concentrations of Cu^{2+} resulted from the change of the quantum photoelectric effect of the QDs.

The quick and sensitive change in color upon increasing concentration of Cu^{2+} indicated the highly efficient analytical application of the easy-to-use "signal off" visual method for semiquantitative and quantitative detection of trace Cu^{2+} by naked eye and scanometric technique, respectively. Figure 3 shows the minimum naked-eye-detectable concentration of Cu^{2+} down to 1.0 × 10^{-8} M and concentration range up to 3.3 × 10^{-4} M. Considering that only 5 μL sample solution was needed, this method could directly read out 5 × 10^{-14} mol of Cu^{2+}. The difference between the color intensities read out from the cyan-blue and yellow channels of Adobe Photoshop software (ΔI) showed a linear relativity to the logarithm of the concentration of Cu^{2+} ranging from 1.0 × 10^{-8} to 3.3 × 10^{-4} M, which followed $\Delta I = -21.0 \log C_{Cu^{2+}} - 72.8$ ($R = 0.99$). The quantitative concentration range was even wider than those with other instrumental analytical methods, such as photoelectrochemical detection (0.02−20.0 μM),[27] fluorescence

dx.doi.org/10.1021/ac401749u | Anal. Chem. 2013, 85, 8735−8740

resonance energy transfer detection (0.16−2.87 μM),[28] atomic absorption spectrometry (0.2−10 μM),[29] and voltammetric detection (0.075−2.5 μM),[30] and 3 orders wider than that of a visual detection method (50−500 μM) reported previously by using functional gold nanoparticles,[31] which showed 5000 times higher detectable limit than the proposed method.

The "signal off" visual method for detection of Cu(II) showed good anti-interference ability due to the copper-induced exciton trapping of QDs. In the presence of 3.3×10^{-5} M different metal cations, all of the spots of NBT/QDs except that for 3.3×10^{-5} M Ag^+ showed the color change from yellow to purple under irradiation of ca. 60 000 lx white light (Figure 5), similar to the irradiation-induced reduction of NBT by QDs

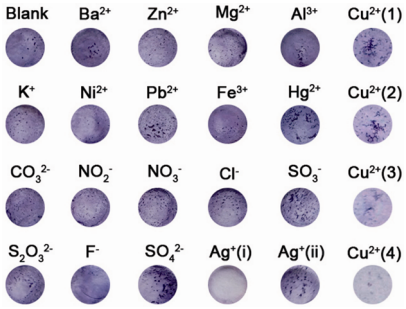

Figure 5. Spots of the QDs and NBT system in the presence of different ions after illumination with white light of ca. 60 000 lx for 5 min. The concentrations of Ag^+ (i) and Ag^+ (ii) are 3.3×10^{-5} and 3.3×10^{-6} M, Cu^{2+} are (1) 1×10^{-8} M, (2) 3.3×10^{-8} M, (3) 3.3×10^{-7} M, and (4) 3.3×10^{-6} M, and other ions are 3.3×10^{-5} M.

in the absence of metal cation (blank in Figure 5); therefore, these metal cations did not interfere with the assay of Cu^{2+}. The interference of Ag^+ resulted from the strong metal−S interaction,[42] which led to the decomposition of QDs.[41] In addition, although the size of the synthesized QDs showed a Poissonian distribution,[25] the distribution did not influence the detection, since the average color intensity at each point was read for quantitative detection.

"Signal on" Visual Detection of CEA. To verify the application of visual quantum photoelectric effect when using QDs as a signal tag, a "signal on" sandwich immunoassay of CEA was designed by using QD-labeled secondary antibody as the probe (Scheme 1C). After the sandwich immunoreaction on the spot coated with capture antibody, the mixture of NBT/QDs dropped on the spot showed dark points after illumination with ca. 60 000 lx white light for 10 min (Figure 6). The dark

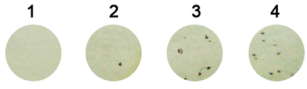

Figure 6. Detecting spots in the presence of 0, 0.02, 0.2, and 2 ng/mL CEA (from 1 to 4) after illumination with white light of ca. 60 000 lx for 10 min.

points could be observed with the naked eye at a CEA concentration down to 0.02 ng/mL (point 2 in Figure 6), while the amount of the dark points increased with the increasing CEA concentration. With the help of Adobe Photoshop software, the area percentages of dark points in the total area could be read out to be 0.3%, 1.5%, and 2.5% at the CEA concentrations of 0.02, 0.2, and 2 ng/mL, respectively. The plot of the percentage vs the logarithm of CEA concentration followed the equation: percentage = 1.5 log c (ng/mL) + 2.8 (R = 0.96). The detection limit of 0.02 ng/mL for this "signal on" visual method was about 20 times lower than the conventional ELISA method, whose detection limit is 0.39 ng/mL.[33] The high sensitivity was attributed to the sensitive quantum photoelectric effect and its convenient visualization. As a proof-of-concept, the nonenzyme visual assay provided a promising platform for the design of multicomponent colorimetric immunoassay. Furthermore, the "signal on" visual method could be simply expanded to the detection of other targets by using QDs as the tag.

CONCLUSIONS

The quantum photoelectric effect of QDs was presented and visualized through the reduction of NBT by photoelectrons escaped from QDs under irradiation. The visual process showed a quick rate due to the highly concentrated energy of excitons, which led to sensitive color change of NBT from yellow to purple. This newly proposed visual strategy for quantum photoelectric effect of QDs could be applied to the design of either "signal off" detection methods, depending on the alternation of the quantum states of the QDs, or "signal on" analytical protocols, using the QDs as a signal tag to monitor the quantum photoelectric effect. These methods could be used for quick detection of trace Cu^{2+} and protein, respectively, by both naked eye and a scanometric technique. The designed methods showed wide concentration range, high sensitivity, and convenient manipulation, indicating promising application. It could be carried out either on solid substrate or in solution for high throughput detection. Therefore, this work extended the application of QDs and could open a new way for visual bioanalysis.

AUTHOR INFORMATION

Corresponding Author

*Phone/Fax: +86-25-83593593. E-mail: hxju@nju.edu.cn.

Notes

The authors declare no competing financial interest.

ACKNOWLEDGMENTS

We gratefully acknowledge National Basic Research Program (2010CB732400) and National Natural Science Foundation of China (21135002, 21121091).

REFERENCES

(1) Curto, A. G.; Volpe, G.; Taminiau, T. H.; Kreuzer, M. P.; Quidant, R.; Hulst, N. F. *Science* **2010**, *329*, 930−933.
(2) Bernevig, B. A.; Hughes, T. L.; Zhang, S. *Science* **2006**, *314*, 1757−1761.
(3) Scholl, J. A.; Koh, A. L.; Dionne, J. A. *Nature* **2012**, *483*, 421−428.
(4) Wang, P.; Ma, X. Y.; Su, M. Q.; Hao, Q.; Lei, J. P.; Ju, H. X. *Chem. Commun.* **2012**, *48*, 10216−10218.
(5) Gill, R.; Zayats, M.; Willner, I. *Angew. Chem., Int. Ed.* **2008**, *47*, 7602−7625.
(6) Pile, D. *Nat. Photonics* **2010**, *4*, 672−673.
(7) Tanne, J.; Schäfer, D.; Khalid, W.; Parak, W. J.; Lisdat, F. *Anal. Chem.* **2011**, *83*, 7778−7785.
(8) Bawendi, M. G.; Steigerwald, M. L.; Brus, L. E. *Annu. Rev. Phys. Chem.* **1990**, *41*, 477−496.
(9) Alivisatos, A. P.; Harris, A. L.; Levinos, N. J.; Steigerwald, M. L.; Brus, L. E. *J. Chem. Phys.* **1988**, *89*, 4001−4011.
(10) Smith, A. M.; Nie, S. *Acc. Chem. Res.* **2010**, *43*, 190−200.

(11) Semonin, O. E.; Luther, J. M.; Choi, S.; Chen, H. Y.; Gao, J.; Nozik, A. J.; Beard, M. C. *Science* **2011**, *334*, 1530−1533.
(12) Cooper, D. R.; Dimitrijevic, N. M.; Nadeau, J. L. *Nanoscale* **2010**, *2*, 114−121.
(13) Xiong, Z.; Zhao, X. S. *J. Am. Chem. Soc.* **2012**, *134*, 5754−5757.
(14) Hao, Q.; Wang, P.; Ma, X. Y.; Su, M. Q.; Lei, J. P.; Ju, H. X. *Electrochem. Commun.* **2012**, *21*, 39−41.
(15) Wang, W. J.; Bao, L.; Lei, J. P.; Tu, W. W.; Ju, H. X. *Anal. Chim. Acta* **2012**, *744*, 33−38.
(16) Yamakoshi, Y.; Umezawa, N.; Ryu, A.; Arakane, K.; Miyata, N.; Goda, Y.; Masumizu, T.; Nagano, T. *J. Am. Chem. Soc.* **2003**, *125*, 12803−12809.
(17) Guertler, C.; Schleder, D. D.; Barracco, M. A.; Perazzolo, L. M. *Aquac. Res.* **2009**, *41*, 1082−1088.
(18) Bieski, B. H. J.; Shiue, G. G.; Bajuk, S. *J. Phys. Chem.* **1980**, *84*, 830−833.
(19) Burkholder, P. R.; Burkholder, L. M.; Almodóvar, L. R. *Bull. Mar. Sci.* **1967**, *17*, 1−15.
(20) Tian, L. F.; Slaughter, D. C. *Comput. Electron. Agric.* **1998**, *21*, 153−168.
(21) Naoghare, P. K.; Kwon, H. T.; Song, J. M. *J. Pharm. Biomed. Anal.* **2010**, *51*, 1−6.
(22) Gómez-Ochoa, P.; Sabate, D.; Homedes, J.; Ferrer, L. *Vet. Immunol. Immunopathol.* **2012**, *146*, 97−99.
(23) Naoghare, P. K.; Kwon, H. T.; Song, J. M. *Biosens. Bioelectron.* **2009**, *24*, 3587−3593.
(24) Chen, Y.; Rosenzweig, Z. *Anal. Chem.* **2002**, *74*, 5132−5138.
(25) Jawaid, A. M.; Chattopadhyay, S.; Wink, D. J.; Page, L. E.; Snee, P. T. *ACS Nano* **2013**, *7*, 3190−3197.
(26) Shen, Y. Y.; Li, L. L.; Lu, Q.; Ji, J.; Fei, R.; Zhang, J. R.; Abdel-Halim, E. S.; Zhu, J. J. *Chem. Commun.* **2012**, *48*, 2222−2224.
(27) Wang, G. L.; Xu, J. J.; Chen, H. Y. *Nanoscale* **2010**, *2*, 1112−1114.
(28) Yang, P.; Zhao, Y.; Lu, Y.; Xu, Q. Z.; Xu, X. W.; Dong, L.; Yu, S. H. *ACS Nano* **2011**, *5*, 2147−2154.
(29) van Staden, J. F.; Hattingh, C. J. *J. Anal. At. Spectrom.* **1998**, *13*, 23−28.
(30) Takeuchi, R.; Santos, A.; Padilha, P.; Stradiotto, N. *Talanta* **2007**, *71*, 771−777.
(31) Zhou, Y.; Wang, S. X.; Zhang, K.; Jiang, X. Y. *Angew. Chem., Int. Ed.* **2008**, *47*, 7454−7456.
(32) Qu, W. S.; Liu, Y. Y.; Liu, D. B.; Wang, Z.; Jiang, X. Y. *Angew. Chem., Int. Ed.* **2011**, *50*, 3442−3445.
(33) Shi, W. T.; Ma, Z. F. *Biosens. Bioelectron.* **2011**, *26*, 3068−3071.
(34) Liu, X.; Cheng, L. X.; Lei, J. P.; Liu, H.; Ju, H. X. *Chem.—Eur. J.* **2010**, *16*, 10764−10770.
(35) Zhou, F.; Wang, M. M.; Yuan, L.; Cheng, Z. P.; Wu, Z. Q.; Chen, H. *Analyst* **2012**, *137*, 1779−1784.
(36) Yang, Z. J.; Zong, C.; Yan, F.; Ju, H. X. *Talanta* **2010**, *82*, 1462−1467.
(37) Deng, S. Y.; Hou, Z. T.; Lei, J. P.; Lin, D. J.; Hu, Z.; Yan, F.; Ju, H. X. *Chem. Commun.* **2011**, *47*, 12107−12109.
(38) Yamazaki, I.; Piette, L. H.; Grover, T. A. *J. Biol. Chem.* **1990**, *265*, 652−659.
(39) Ge, C. W.; Xu, M.; Liu, J.; Lei, J. P.; Ju, H. X. *Chem. Commun.* **2008**, 450−452.
(40) Jiang, X.; Xie, Y.; Lu, J.; He, W.; Zhu, L.; Qian, Y. *J. Mater. Chem.* **2000**, *10*, 2193−2196.
(41) Cheng, L. X.; Liu, X.; Lei, J. P.; Ju, H. X. *Anal. Chem.* **2010**, *82*, 3359−3364.
(42) Goates, J. R.; Gordon, M. B.; Faux, N. D. *J. Am. Chem. Soc.* **1952**, *74*, 835−836.